Yang, L. & Gómez García, R. 2022, "Input-absorptive high-order wideband balun bandpass filters with quasi-elliptic-type response", in 2022 52th European Microwave Conference (EuMC), Milan, Italy, 2022, pp. 333-336.

Available at http://dx.doi.org/10.23919/EuMC54642.2022.9924468

Input-Absorptive High-Order Wideband Balun Bandpass Filters With Quasi-Elliptic-Type Response

Li Yang[#1], Roberto Gómez-García[#2]

[#]Department of Signal Theory and Communications, University of Alcalá, Alcalá de Henares, Madrid, 28871, Spain

[1]li.yang@uah.es, [2]roberto.gomez.garcia@ieee.org

***Abstract* — A class of input-reflectionless high-order wideband balun bandpass filters (BPFs) with quasi-elliptic-type response are reported. They consist of two main circuit parts: 1) a three-port reflective-type high-order balun BPF network and 2) a resistively-terminated microstrip T-junction that is shunt connected at the unbalanced port. The reflective-type balun BPFs developed with 5th- and 6th-order Chebyshev equal-ripple responses are firstly described. By replacing the last two virtually-short-circuit-ended quarter-wavelength transmission-line (TL) stubs with open-circuit-ended half-wavelength TL stubs, their balun counterparts with two close-to-passband transmission zeros (TZs) are then presented. As design example, a 5th-order input-reflectionless quasi-elliptic-type wideband balun BPF is theoretically discussed. Furthermore, for experimental-validation purposes, a proof-of-concept two-layer microstrip prototype of 5th-order balun BPF is simulated and tested. Its measured metrics are 2.05-GHz center frequency, 3-dB fractional bandwidth of 63.61% for the two output ports, input-power-matching levels higher than 10 dB, and stopband-power-rejection levels above 26.1 dB from DC to 5 GHz.**

***Keywords* — Absorptive filter, balun, bandpass filter (BPF), multilayer circuit, reflectionless filter, transmission zero (TZ), vertical transition, wideband filter.**

I. Introduction

Absorptive/reflectionless bandpass filters (BPFs) are playing an important role in RF front-end chains of modern communication systems. Compared with traditional reflective-type BPFs, their counterparts featured with absorptive-type properties bring guarantees of higher stability for the adjacent active components [1]. Specifically, the non-transmitted RF-power echoes from reflective-type BPFs introduce harmful intermodulation products, which are generally suppressed by bulky RF isolators [2]. However, absorptive BPFs can consume most of the unwanted stopband RF-power reflections at the resistive elements included inside themselves [3]. Until now, reflectionless BPFs and filtering circuits have been developed by using three main different approaches or structures as in [4]–[9]. In [4], by means of properly-designed equal-amplitude but out-of-phase even- and odd-mode equivalent circuits, a class of reflectionless filters with theoretically-perfect input and output power matching at all frequencies was devised. In [5], a quasi-absorptive BPF response was obtained by inserting 4th-order BPF units between two back-to-back-cascaded quadrature couplers whose isolated ports were loaded by 50-Ω resistors. In addition, based on complementary-diplexer bandpass-bandstop topologies, input-/two-port-reflectionless narrowband BPFs, wideband BPFs, and wideband balun BPFs were studied in [6]–[9], respectively. In [7], a two-layer wideband balun BPF with broadband input-absorptive behavior was designed with three-port microstrip-to-slotline transitions and a shunt 50-Ω-ended microstrip line. However, it suffered from passband-rounded responses as a major drawback. Hence, to improve passband flatness, selectivity, and the stopband-power-absorption-ratio profile, an input-reflectionless wideband balun BPF with four-pole quasi-elliptic-type filtering response was designed in [9]. Nevertheless, for the balun BPFs devised in [7] and [9], there is no discussion about how to achieve higher-order wideband balun BPFs with broadband input-reflectionless behavior.

In this paper, based on the input-reflectionless 4th-order quasi-elliptic-type wideband balun BPF reported in [9], a class of high-order wideband balun BPFs is engineered. Firstly, their building reflective-type balun BPF networks for the cases of 5th- and 6th-order Chebyshev equal-ripple responses are analyzed. Later, their input-reflectionless quasi-elliptic-type counterparts are shown. For illustration purposes, the design procedure of a 5th-order input-reflectionless quasi-elliptic-type wideband balun BPF is detailed. Finally, for experimental-validation purposes, a two-layer input-reflectionless 5th-order balun BPF microstrip prototype is manufactured and measured.

II. Analysis and Design

The generalized transmission-line (TL) equivalent circuit of the proposed input-reflectionless high-order wideband balun BPF is depicted in Fig. 1. The conceived wideband balun BPF in Fig. 1(a) consists of two parts: 1) a three-port (N+3)th-order reflective-type balun BPF network with $N \geq 1$ and 2) a shunt resistively-terminated T-junction loaded at the unbalanced port (Port 1) which acts as the absorptive network. Herein, this (N+3)th-order reflective-type balun BPF network can be viewed as the third-order design in [10] cascaded with 2N pairs of in-series TL segments and shunt virtually-short-circuit-ended TL stubs, which results in a (N+3)th-order Chebyshev equal-ripple filtering response. Besides, by optionally replacing the last two virtually-short-circuit-ended stubs with two open-circuit-ended stubs, a (N+3)th-order Chebyshev equal-ripple filtering response with two close-to-passband transmission zeros (TZs) for the quasi-elliptic-type balun BPF network is attained. The design impedances of the open-circuit-ended stub, the short-circuit-ended stubs, the cascaded TL segments, the N pairs of in-series TL segments, and the N pairs of shunt virtually-short-circuit-ended stubs are Z_m, Z_s, Z_1, Z_{11}, Z_{21}, …, Z_{N1}, and Z_{12}, Z_{22}, …, Z_{N2}, respectively. The line impedances of the optional

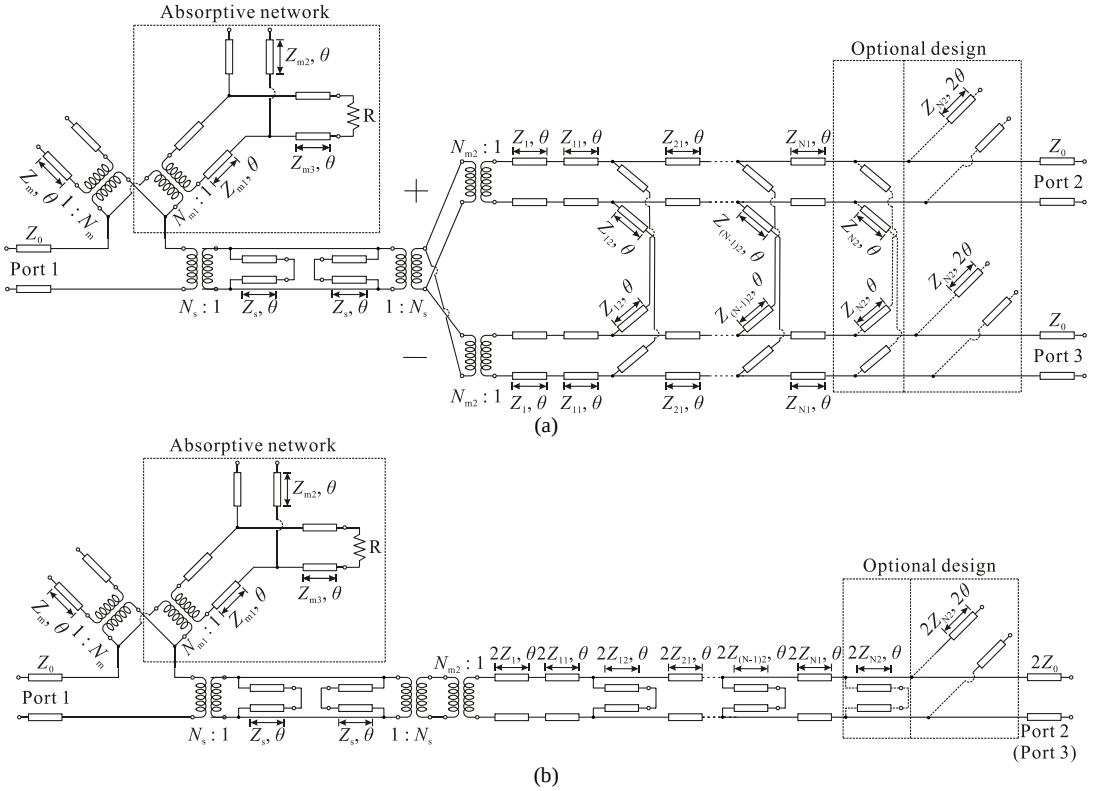

Fig. 1. Generalized transmission-line (TL) equivalent circuit of the proposed input-reflectionless high-order wideband balun BPF. (a) Three-port wideband balun BPF composed of a (*N*+3)th-order reflective-type balun network and a shunt resistively-terminated T-junction. (b) Associated two-port 50-to-100-Ω wideband impedance transformer.

pair of shunt open-circuit-ended stubs are also assumed to be Z_{N2}. For the resistively-terminated T-junction, the impedance variables of its cascaded TL segments and shunt open-circuit-ended stub are Z_{m1}, Z_{m3}, and Z_{m2}, respectively. Z_0 is the reference port impedance and R is the resistance of the resistor. Most of these stubs and TL segments are set to have the same electrical length θ (i.e., quarter-wavelength-long at the center frequency f_0), except the electrical lengths of the optional open-circuit-ended stubs that are assumed to be 2θ. Moreover, note that four transformers with different turns ratios of N_m, N_s, N_{m1}, and N_{m2} are used to properly model the impedance variations of the coupled microstrip and slotline resonators arising in the practical electromagnetic (EM) simulation.

Next, the properties of the proposed balun BPF are theoretically determined with its modified two-port equivalent circuit in Fig. 1(b). As can be seen, it is a 50-to-100-Ω wideband impedance transformer, in which the impedance values of its building elements (i.e., the cascaded TL segments, the N in-series TL segments, the virtually-short-circuit-ended stubs, the optional open-circuit-ended stub, and the output port) are doubled. Through the constituent *ABCD* matrices of this two-port 50-to-100-Ω network, its power transmission (S_{21}) and reflection (S_{11}) coefficients are derived to be as follows:

$$S_{21} = \frac{2\sqrt{z_{01}z_{02}}}{Az_{02} + B + Cz_{01}z_{02} + Dz_{01}} \tag{1}$$

$$S_{11} = \frac{Az_{02} + B - Cz_{01}z_{02} - Dz_{01}}{Az_{02} + B + Cz_{01}z_{02} + Dz_{01}} \tag{2}$$

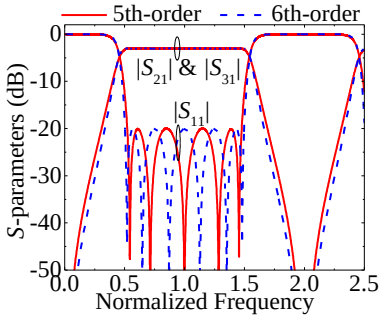

Fig. 2. Theoretical power transmission ($|S_{21}|$) and reflection ($|S_{11}|$) responses of the proposed reflective-type wideband balun BPF when N =2 and 3 for (i) a 5th-order Chebyshev equal-ripple response (Z_m = 1.004Z_0, Z_s = 1.6468Z_0, Z_1 = 0.824Z_0, Z_{11} = 1.146Z_0, Z_{12} = 2.252Z_0, Z_{21} = 0.982Z_0, and Z_{22} = 1.884Z_0) and (ii) a 6th-order Chebyshev equal-ripple response (Z_m = 0.967Z_0, Z_s = 1.6858Z_0, Z_1 = 0.834Z_0, Z_{11} = 1.177Z_0, Z_{12} = 2.029Z_0, Z_{21} = 1.035Z_0, Z_{22} = 1.953Z_0, Z_{31} = 0.9382Z_0, and Z_{32} = 2.159Z_0).

where z_{01} and z_{02} are the normalized input and output port impedances, and the characteristic function F_M is formulated as

$$F_M = \frac{S_{11}}{S_{21}} = \frac{(Az_{02} - Dz_{01}) + (B - Cz_{01}z_{02})}{2\sqrt{z_{01}z_{02}}} \tag{3}$$

where Az_{02}-Dz_{01} and B-$Cz_{01}z_{02}$ are the real and imaginary parts of this F_M function, respectively.

A. 5th-/6th-Order Reflective-Type Balun BPFs

By initially choosing the virtually-short-circuit-ended stubs, the frequency responses of the reflective-type wideband balun BPF are firstly discussed for the case $N_m = N_s = N_{m1} = N_{m2} = 1$.

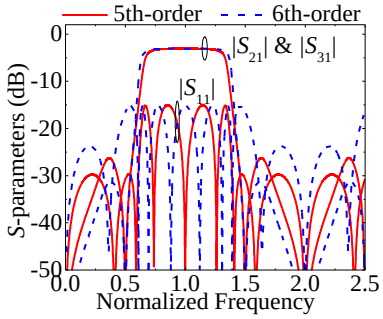

Fig. 3. Theoretical power transmission ($|S_{21}|$ and $|S_{31}|$) and input-reflection ($|S_{11}|$) responses of the proposed input-reflectionless quasi-elliptic-type wideband balun BPFs when N = 2 and 3 for (i) a 5th-order Chebyshev equal-ripple responses (Z_m = 1.1463Z_0, Z_s = 0.9261Z_0, Z_1 = 1.1882Z_0, Z_{11} = 1.4393Z_0, Z_{12} = 0.5261Z_0, Z_{21} = 0.8572Z_0, Z_{22} = 1.9074Z_0, Z_{m1} = 1.665Z_0, Z_{m2} = 1.5728Z_0, and Z_{m3} = 1.1586Z_0), and (ii) a 6th-order Chebyshev equal-ripple response (Z_m = 1.1126Z_0, Z_s = 1.086Z_0, Z_1 = 1.1182Z_0, Z_{11} = 1.339Z_0, Z_{12} = 0.4726Z_0, Z_{21} = 0.9178Z_0, Z_{22} = 1.1166Z_0, Z_{31} = 0.9074Z_0, Z_{32} = 2.214Z_0, Z_{m1} = 1.839Z_0, Z_{m2} = 1.139Z_0, and Z_{m3} = 1.3494Z_0).

Here, the corresponding two-port impedance transformer is designed to exhibit a (N+3)th-order Chebyshev equal-ripple filtering response with passband ripple L_A = 0.044 dB and electrical length θ_c = 46.98° at the lower cut-off frequency f_c = 1.044 GHz (i.e., in-band return-loss level of 20 dB at f_0 = 2 GHz). From the design specifications, the impedance values of the 5th- and 6th-order two-port reflective-type wideband 50-to-100-Ω networks with N = 2 and 3 are theoretically determined, where the imaginary parts of their characteristic functions F_M are forced to be equal to zero with B-$Cz_{01}z_{02}$ = 0. The calculated Chebyshev equal-ripple responses of the 5th- and 6th-order wideband balun BPFs with the same in-band performance are plotted in Fig. 2, which attests the effectiveness of the proposed equivalent circuits for high-order wideband balun BPF design.

B. Input-Reflectionless Quasi-Elliptic-Type Balun BPFs

By selecting the open-circuit-ended half-wavelength stubs as the last design elements, two close-to-passband transmission zeros (TZs) can be produced in the above-discussed balun BPFs. Based on the two-port 50-to-100-Ω network with the shunt resistively-terminated TL T-junction loaded at the input port (Port 1) as shown in Fig. 1(b), a class of input-reflectionless high-order balun BPFs can be synthetically designed with arbitrary Chebyshev equal-ripple responses. Here, as depicted in Fig. 3, input-reflectionless 5th- and 6th-order quasi-elliptic-type wideband balun BPF responses with the same equal-ripple power-matching levels but different bandwidths are demonstrated. For illustration purposes, the design procedure of the input-reflectionless 5th-order balun BPF depicted in Fig. 3 is summarized. Based on its relevant 5th-order two-port input-reflectionless 50-to-100-Ω wideband network in Fig. 1(b) with (1)–(3), $R = Z_0$, and $N_m = N_s = N_{m1} = N_{m2} = 1$, its complex F_M is firstly obtained. Meanwhile, due to the employed shunt half-wavelength open-circuit-ended stubs, two close-to-passband TZs to attain a quasi-elliptic-type response are produced at $f_0/2$ and $3f_0/2$, respectively. Then, with the imaginary part of the input impedance of the lossy TL T-junction, a 5th-order reflective-type wideband Chebyshev equal-ripple response

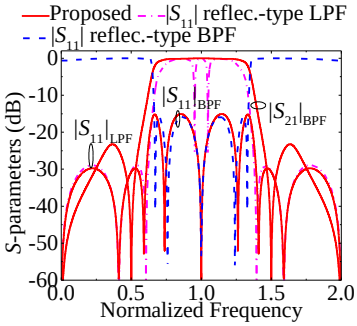

Fig. 4. Theoretical power transmission ($|S_{21}|$) and input-reflection ($|S_{11}|$) responses of (i) the proposed two-port input-reflectionless 5th-order 50-to-100-Ω quasi-elliptic-type impedance transformers (Z_m = 1.1463Z_0, Z_s = 0.9261Z_0, Z_1 = 1.1882Z_0, Z_{11} = 1.4393Z_0, Z_{12} = 0.5261Z_0, Z_{21} = 0.8572Z_0, Z_{22} = 1.9074Z_0, Z_{m1} = 1.665Z_0, Z_{m2} = 1.5728Z_0, and Z_{m3} = 1.1586Z_0), (ii) its reflective-type 5th-order $|S_{11}|$ associated to the real part of F_M for attaining the specified Chebyshev equal-ripple BPF response (Z_m = 1.1463Z_0, Z_s = 0.9261Z_0, Z_1 = 1.1882Z_0, Z_{11} = 1.4393Z_0, Z_{12} = 2.252Z_0, Z_{21} = 0.8572Z_0, Z_{22} = 1.9074Z_0, Z_{m1} = 1.5357Z_0, Z_{m2} = 1.7728Z_0, and Z_{m3} = 1.1586Z_0), and (iii) the reflective-type 5th-order $|S_{11}|$ resulting from the imaginary part of characteristic function of the reshaped input-reflectionless LPF network to meet the specified Chebyshev equal-ripple LPF response (Z_m = 1.1894Z_0, Z_s = 0.9261Z_0, Z_1 = 1.1882Z_0, Z_{11} = 1.4393Z_0, Z_{12} = 0.5261Z_0, Z_{21} = 0.8572Z_0, Z_{22} = 1.9074Z_0, Z_{m1} = 1.665Z_0, Z_{m2} = 1.5728Z_0, and Z_{m3} = 1.1586Z_0).

associated to the real part of the recalculated F_M is targeted with passband ripple L_{A1} = 0.1156 dB and electrical length θ_{c1} = 59.76° at the lower cut-off frequency f_{c1} = 1.328 GHz (i.e., in-band return-loss power-matching levels above 15.8 dB within a relative bandwidth of 67.2% in relation to f_0 = 2 GHz). On the other hand, by removing the terminating resistor of the TL T-junction and by ending the output port of the 5th-order reflective-type 50-to-100-Ω channel with a 50-Ω resistor, the initial lossy 5th-order wideband BPF network is reshaped as a lossy 5th-order low-pass filter (LPF). Similarly, with the imaginary part of the input impedance of the resistively-terminated 50-to-100-Ω channel, a fifth-order reflective-type Chebyshev equal-ripple response resulting from the imaginary part of the characteristic function of the reshaped lossy LPF network is designed to meet a passband ripple L_{A2} = 0.005649 dB for an electrical length θ_{c2} = 56.07° at the cut-off frequency f_{c2} = 1.246 GHz. Finally, as depicted in Fig. 4 and to simultaneously attain these specified reflective-type 5th-order wideband BPF and LPF Chebyshev equal-ripple responses, the impedance values of the input-reflectionless two-port 5th-order quasi-elliptic-type wideband 50-to-100-Ω network are quantitatively derived. As observed, compared with the resulting values for the impedances of the reshaped 5th-order lossy LPF, only the Z_m value in the input-absorptive 5th-order wideband balun BPF is slightly adjusted.

III. Simulation and Measurement

For practical-validation purposes, a proof-of-concept input-reflectionless 5th-order quasi-elliptic-type wideband balun BPF is developed and tested in a two-layer substrate. Its devised layout is shown in Fig. 5, and a substrate with relative dielectric constant ε_r = 10.2, dielectric thickness h = 1.27 mm, and dielectric loss tangent tan(δ_D) = 0.0023 is used. Here, the constituent stubs and TL segments in Fig. 1 with N = 2 are

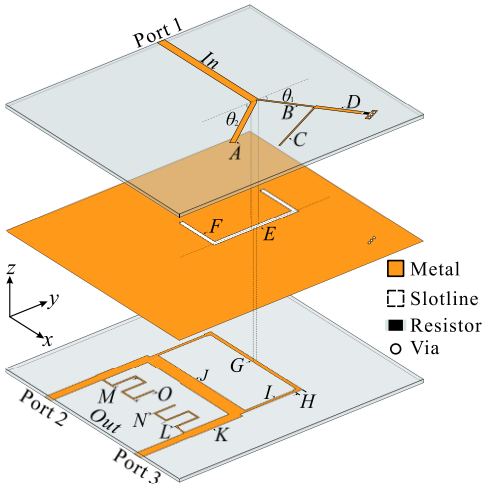

Fig. 5. Layout of the developed input-reflectionless 5th-order quasi-elliptic-type wideband balun prototype with design dimensions: L_{In} = 25, L_A = 14.26, L_B = 14.84, L_C = 14.75, L_D = 14.28, L_E = 16.5, L_F = 6.45, L_G = 28.19, L_H = 0.935, L_I = 14.6, L_J =25.98, L_K = 13.82, L_L = 2.59, L_M = 8.31, L_N =3.565 , L_O = 7, L_{Out} = 10, W_{In} = W_{Out} = 1.1, W_A = 0.83, W_B = 0.25, W_C = 0.28, W_D = 0.77, W_E = W_F = 0.48, W_G = W_H = 0.72, W_I = 0.42, W_J = 3.41, W_K = 1.39, W_L = W_M = W_N = W_O = 0.14 (unit: mm), θ_1 = 75°, and θ_2 = 45°.

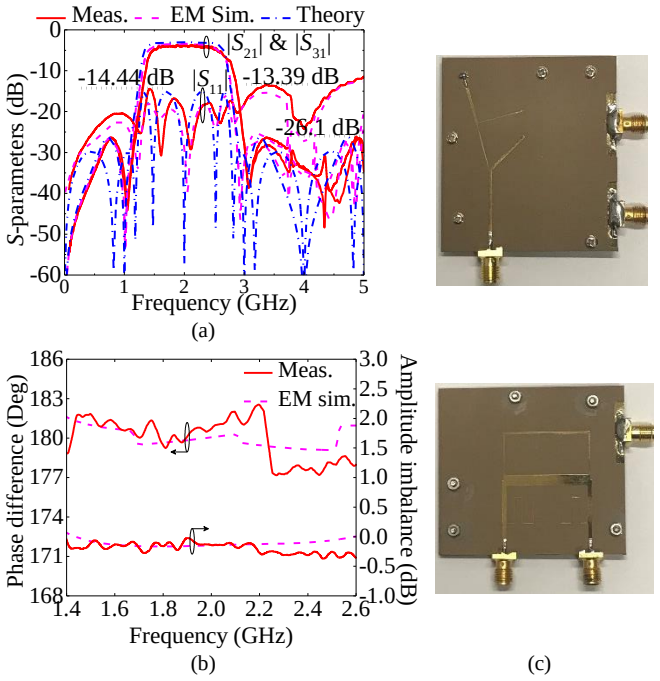

Fig. 6. Manufactured input-reflectionless 5th-order quasi-elliptic-type wideband balun BPF whose layout is given in Fig. 5. (a) Theoretical, simulated, and measured power transmission ($|S_{21}|$ and $|S_{31}|$) and input-reflection ($|S_{11}|$) responses. (b) Simulated and measured amplitude imbalance and phase difference. (c) Photographs (top/bottom view) of the assembled prototype.

correspondingly represented by the microstrip and slotline resonators. In order to avoid the unwanted coupling between the slotline and the virtually-short-circuit-ended microstrip lines, a folded U-slot structure is chosen. In addition, meandered half-wavelength open-circuit-ended microstrip lines are used to achieve a compact circuit size. The measured resistance of the soldered resistor is 50.1 Ω. Fig. 6 depicts the simulated and measured results, along with the photographs of the built 5th-order wideband balun BPF. As shown in Fig. 6(a), a close agreement between the theoretical, simulated, and measured responses is obtained. The main measured performance metrics of this wideband balun BPF are as follows: 2.05-GHz center frequency, 3-dB bandwidth from 1.398 GHz to 2.702 GHz (i.e., 63.61% in fractional terms) for both output ports, input-power-matching levels above 10 dB, and stopband-power-rejection levels higher than 26.1 dB from DC to 5 GHz. Fig. 6(b) reveals a measured in-band amplitude imbalance below 0.31 dB and phase difference less than 2.81°. The measured minimum in-band power-absorption ratio is 14.49% at 1.882 GHz.

IV. Conclusion

A class of high-order input-reflectionless quasi-elliptic-type wideband balun BPFs has been reported. With the proposed TL equivalent circuits, the reflective-type baluns with 5th- and 6th-order Chebyshev equal-ripple responses are firstly discussed. Afterwards, their 5th- and 6th-order input-reflectionless quasi-elliptic-type counterparts are presented. As practical validation, a two-layer input-reflectionless 5th-order quasi-elliptic-type balun prototype is designed, manufactured, and characterized.

Acknowledgment

This work has been supported in part by the GOT ENERGY TALENT (GET) fellowship programme cofunded by the EU as part of the H2020-MSCA-COFUND programme under Grant Agreement number 754382 and in part by the Spanish Ministry of Science and Innovation (State Research Agency) under Project PID2020-116983RB-I00.

References

[1] Mini-Circuits, Brooklyn, NY., "Reflectionless filters improve linearity and dynamic range," *Microw. J.*, vol. 58, no. 8, pp. 42–50, Aug. 2015.

[2] R. Gómez-García, D. Psychogiou, J.-M. Muñoz-Ferreras, and L. Yang, "Avoiding RF isolators: Reflectionless microwave bandpass filtering components for advanced RF front ends," *IEEE Microw. Mag.*, vol. 21, no. 12, pp. 68–86, Dec. 2020.

[3] M. A. Morgan, "Think outside the band: Design and miniaturization of absorptive filters," *IEEE Microw. Mag.*, vol. 19, no. 7, pp. 54–62, Nov. 2018.

[4] M. A. Morgan and T. A. Boyd, "Theoretical and experimental study of a new class of reflectionless filter," *IEEE Trans. Microw. Theory Techn.*, vol. 59, no. 5, pp. 1214–1221, May. 2011.

[5] P. Ma, B. Wei, Y. Heng, C. Luo, X. Guo, and B. Cao, "Design of absorptive superconducting filter," *Electron. Lett.*, vol. 53, no. 11, pp. 728–730, May 2017.

[6] D. Psychogiou and R. Gómez-García, "Reflectionless adaptive RF filters: Bandpass, bandstop, and cascade designs," *IEEE Trans. Microw. Theory Techn.*, vol. 65, no. 11, pp. 4593–4605, Nov. 2017.

[7] L. Yang, R. Gómez-García, J.-M. Muñoz-Ferreras, and W. Feng, "Multilayered wideband balun bandpass filters designed with input-reflectionless response," in *Proc. 49th Eur. Microw. Conf.*, Paris, France, Oct. 1–3, 2019, pp. 452–455.

[8] L. Yang et al., "Multilayered reflectionless wideband bandpass filters with shunt/in-series resistively terminated microstrip lines," *IEEE Trans. Microw. Theory Techn.*, vol. 68, no. 3, pp. 877–893, Mar. 2020.

[9] L. Yang, R. Gómez-García, M. Fan, and R. Zhang, "Multilayered input-reflectionless quasi-elliptic-type wideband bandpass filtering devices on diplexer-based structures," *IEEE Trans. Microw. Theory Techn.*, vol. 70, no. 1, pp. 122–138, Jan. 2022.

[10] L. Yang, L. Zhu, W.-W. Choi, K.-W. Tam, R. Zhang, and J. Wang, "Wideband balanced-to-unbalanced bandpass filters synthetically designed with Chebyshev filtering response," *IEEE Trans. Microw. Theory Techn.*, vol. 66, no. 10, pp. 4528–4539, Oct. 2018.